Article

Using Discrete Multiphysics Modelling to Assess the Effect of Calcification on Hemodynamic and Mechanical Deformation of Aortic Valve

Adamu Musa Mohammed[1, 3,*], Mostapha Ariane[2], Alessio Alexiadis[1]

[1] School of Chemical Engineering, University of Birmingham, B15 2TT, Birmingham, United Kingdom; ammohd@atbu.edu.ng, amm702@bham.ac.uk (A.M.M.); A.Alexiadis@bham.ac.uk (A.A.)

[2] Department of Materials and Engineering, Sayens - University of Burgundy, Dijon, France; Mostapha.Ariane@u-bourgogne.fr (M.A.)

[3] Department of Chemical Engineering, Faculty of Engineering and Engineering Technology, Abubakar Tafawa Balewa University Bauchi, Nigeria; ammohd@atbu.edu.ng, amm702@bham.ac.uk (A.M.M.)

***** Correspondence: ammohd@atbu.edu.ng; Tel.: +44 (0) 776 717 3356

Received: date; Accepted: date; Published: date

Abstract: This study proposes a 3D particle-base (discrete) multiphysics approach for modelling calcification in the aortic valve. Different stages of calcification (from mild to severe) were simulated, and their effect on the cardiac output assessed. The cardiac flow rate decreases with the level of calcification. In particular, there is a critical level of calcification below which the flow rate decreases dramatically. Mechanical stress on the membrane is also calculated. The results show that, as calcification progresses, spots of high mechanical stress appear. Firstly, they concentrate in the regions connecting two leaflets; when severe calcification is reached, then they extend to the area at the basis of the valve.

Keywords: Discrete Multiphysics Modelling; Smoothed Particle Hydrodynamics; Lattice Spring Model; Particle-base method; Aortic Valve; Calcification; Stenosis

1. Introduction

Aortic valve disease is the malfunction of the aortic valve due to heart malformation at birth (congenital) or developed during a lifetime related to injury, age, or calcification of the valve [1]. Calcification, in particular, may result in calcific aortic valve disease (CAVD) caused by calcium deposits on the valve leaflets, which affects mainly the elderly population with an incidence rate of 2 – 7% in the population above 65 years of age [2]. Over time, calcium build-up makes the aortic valve stiffer preventing full opening (stenosis) and hindering the blood flow from the left ventricle to the aorta. It may also prevent the valve from closing properly (regurgitation) resulting in blood leakages back to the ventricle.

Stenosis starts with the risk of leaflet deformation and progresses from early lesions to valve obstruction, which is initially mild to moderate but eventually becomes severe, with or without clinical symptoms [3] and the patient has high risk of cardiac failure.

In the literature, several studies focus on the dynamics of blood flow and the deformation of the calcified aortic valve leaflets to better understand and assess the severity of calcification. Computational fluid dynamics (CFD) was used to generate patient-specific aortic valve models from

patient's medical images by [4] and [5]. Other studies focus [6–10] on investigating the stresses on the valve leaflets excluding the fluid flow behaviour in the model. Since the behaviour of the aortic valve depends on both the fluid and the leaflets, a fluid-structure interaction (FSI) approach is recommended to model the complex dynamic of this problem [2,11].

In this paper, we use Discrete Multi-Physics (DMP) [12–14] to develop a 3D model representing various stages of a calcification of the aortic valve. DMP has been extensively used in-silico medicine for modelling a variety of human systems including the aortic valve [15], the intestine [16], deep venous valves [17,18], the lungs [19] and, in conjunction with Machine Learning, peristalsis in the oesophagus [20].

2. The model

As mentioned, the multiphysics model used in this study is based on DMP, a computational method that combines various particle methods. In the case under investigation, the computational domain is divided into two parts: (i) a liquid part (blood) where Smooth Particle Hydrodynamics (SPH) is used, and (ii) the solid structure part (valve) where stress deformation equation is solved using the Lattice Spring Model (LSM). The two parts are coupled together to represent an FSI model that simulate the valve deformation and blood flow dynamics within the valve. The reader can refer to [21] for an introduction to SPH, to [22] for an introduction to LSM, and to [12,13] for details on how to link the two models together in DMP.

In Figure 1a, the valve's leaflets (tricuspid) are shown; Figure 1b shows the overall geometry. The geometry was firstly designed as a CAD model (nodes and elements) and then transformed to a particle model as explained in the Appendix. Simulations were run with the Open source code LAMMPS [23].

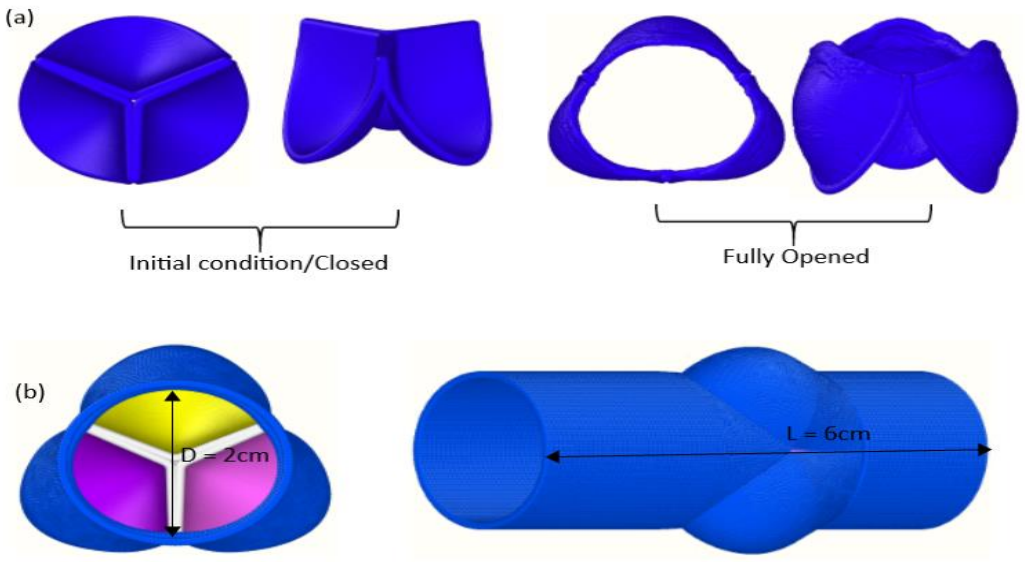

Figure 1. Valve leaflets (a) and complete geometry (b)

The system is 3-dimensional and consists of 418,743 particles: 342,358 particles for the fluid, 19,725 particles for the leaflets and 56,660 particles for the rigid pipe.

Peer-reviewed version available at *ChemEngineering* **2020**, *4*, 48; doi:10.3390/chemengineering4030048

Table 1. Model parameters used in the simulation, for the meaning of SPH parameters such as α or *h*, refer to Liu and Liu, 2003[21].

Parameters	Notation	Values
Length	L	$6 \cdot 10^{-2}$ m
Diameter	D	$2 \cdot 10^{-2}$ m
Initial Particle spacing	l	$0.4 \cdot 10^{-3}$ m
Blood Density	ρ	1060 kg/m^3
Frequency	f	1.167 s^{-1} (70 beats min^{-1})
Dynamic viscosity	μ	0.003 Pa·s
Elastic constant	k	10 -14500 N m^{-1}

In the simulation, the flow is driven by a periodic acceleration (Figure 2) given by

$$G = G_0 \sin^n(\omega t) cos(\omega t - \phi) \quad (1)$$

where G_0=400 ms^{-2}, $\omega = 2\pi f$ is the angular frequency, $n = 13$ and $\phi = \pi/10$ as discussed in Stevens et al., 2003. The value of G_0 is determined to achieve full opening of the valve that gives an average flow rate around 600 mL s^{-1} for valves at normal condition, which is consistent with the literature e.g. [24–26].

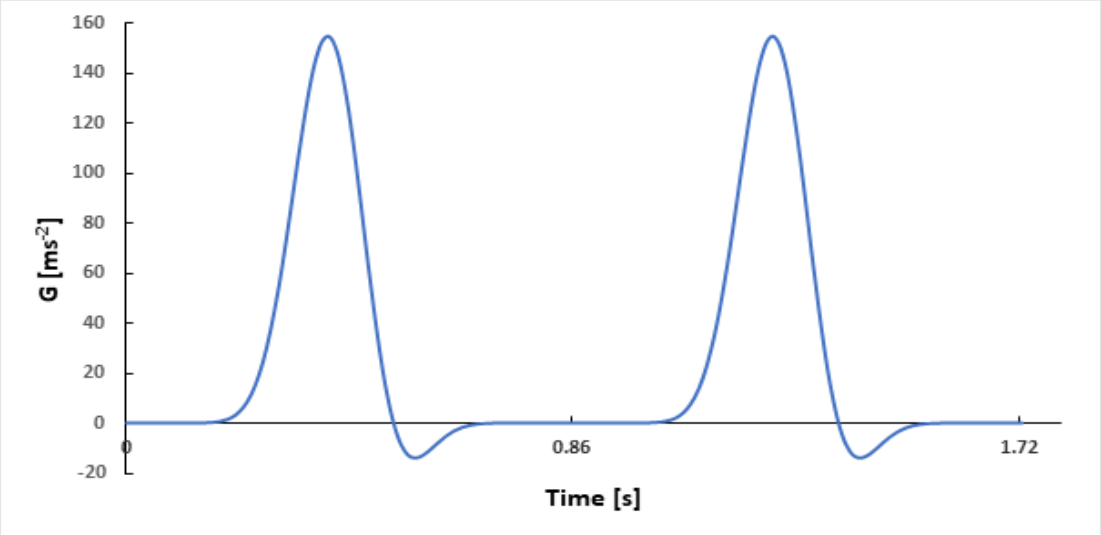

Figure 2. Pulsatile flow function

As mentioned, the flexible valve is modelled with LSM, which is a common approach for cardiovascular valves [27]. This implies that each computational particle is linked with its neighbour particles by means of a force such as

$$F = k(r - r_0) \tag{2}$$

where r_0 is the initial distance between the two particles, r the distance at time t and k a Hookean constant. In LSM, the value of k is linked to the Young modulus E of the material [28]. In practice, however, it is not always straightforward to calculate k from E in the case of complex geometries, in particular, with irregular particles distribution [29]. For this reason, we use a more practical approach: k is determined, together with G_0, in such a way that the valve opens fully and the flow rate for a healthy and non-calcified valve, is 600 mL s^{-1} as discussed above.

3. Results and Discussion

3.1. Stages of calcification

In our model, the value of k was chosen to control the stiffness of the valve and model calcification. The higher the value of k, the stiffer the valve. In our model, higher values of k are used to model a higher degree of calcification. We define the degree of calcification γ as

$$\gamma = \log\left(\frac{k}{k_H}\right) \tag{3}$$

where k is the spring constant used to simulate the calcified valve and kH is the stiffness of the healthy valve. Figure 3 shows the valve during maximal opening for four different degrees of calcification.

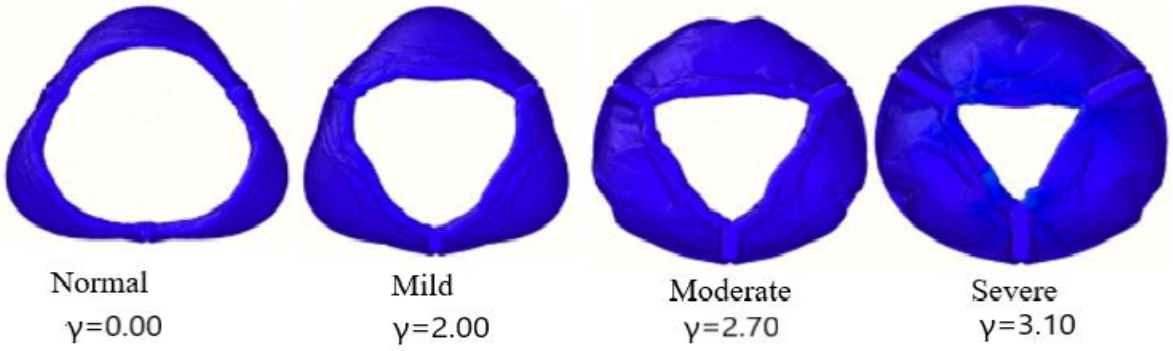

Figure 3. Severity of aortic valve stenosis in terms of orifice opening (stenosis)

Some important parameters like flow velocity, volume flow rate as well as stress can be used to ascertain the level of calcification of the valves. Figure 4 shows how the flow velocity in the valve is affected by calcification.

Peer-reviewed version available at *ChemEngineering* **2020**, *4*, 48; doi:10.3390/chemengineering4030048

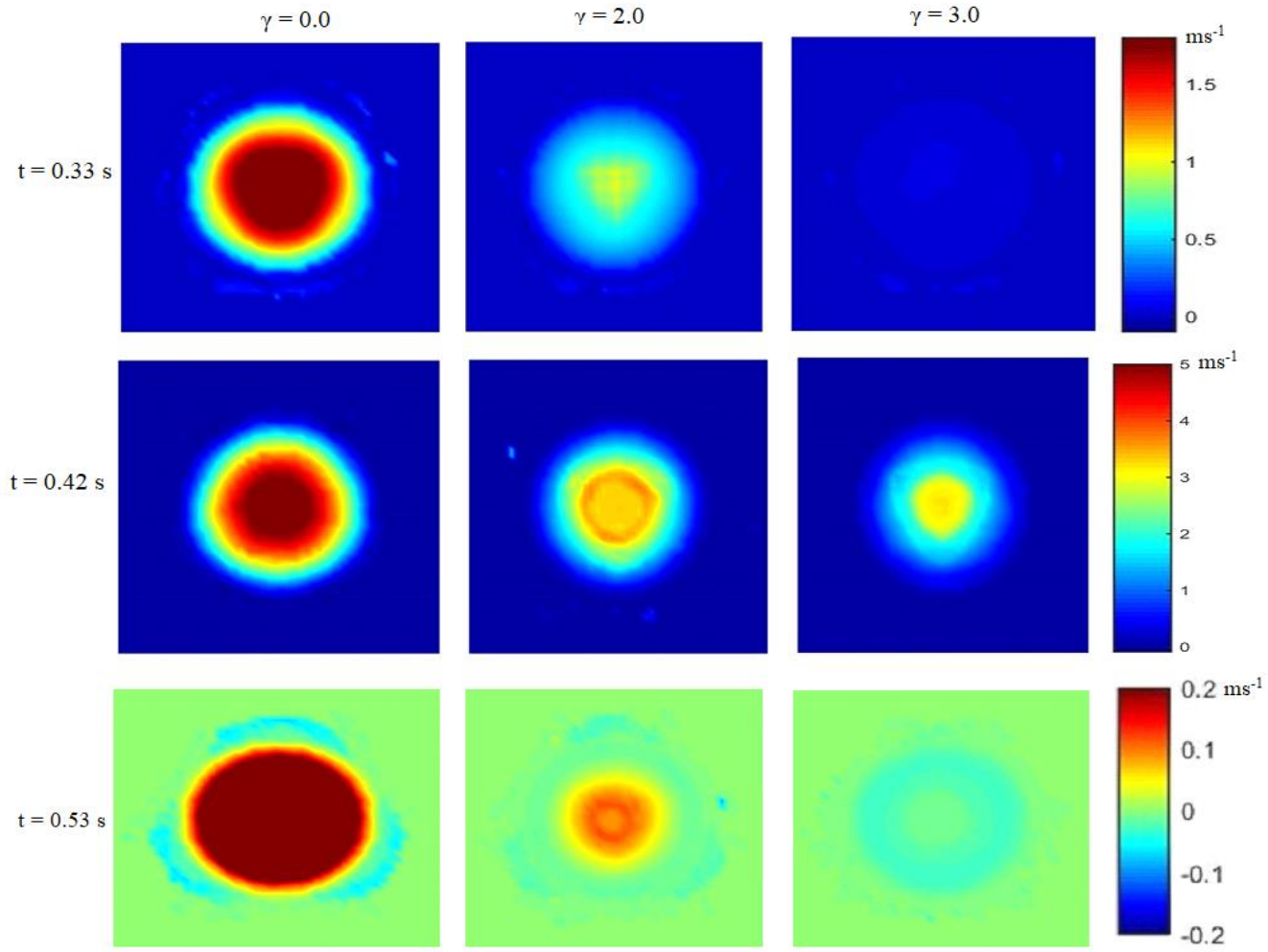

Figure 4. Velocity profile at different time steps

The flow velocity was measured on a section just above the valve, for three different degrees of calcification, and three different times. According to the level of calcification the valve opens and closes at different times. The healthy valve (γ=0) starts opening at $t = 0.29$ s, reaches maximal opening (peak systole) at $t = 0.41$ s and closes again at $t = 0.56$ s. The valve with γ=2.0 starts opening at $t = 0.32$ s, reaches maximal opening at $t = 0.43$ s and closes again at $t = 0.54$ s. The valve with γ=3.0 starts opening at $t = 0.37$ s, reaches maximal opening at $t = 0.43$ s and closes again at $t = 0.53$ s. Figure 4 also relates with Figure 3 in showing how the valve opening is reduced (stenosis) in case of calcification. The time to attain peak velocity varies with the severity of the valve's stenosis, which is associated with high mortality risk and the need for aortic replacement [30]. The time at which the valve closes also varies with the severity of calcification; at γ=3.0 there is also evidence of regurgitation (back flow) a characteristic of a stenotic aortic valve [2,3,9]. Figure 4 also shows that, as expected, the blood flow in the healthy valve (γ=0.0) is higher than in the calcified valves (γ=2.0 and γ=3.0).

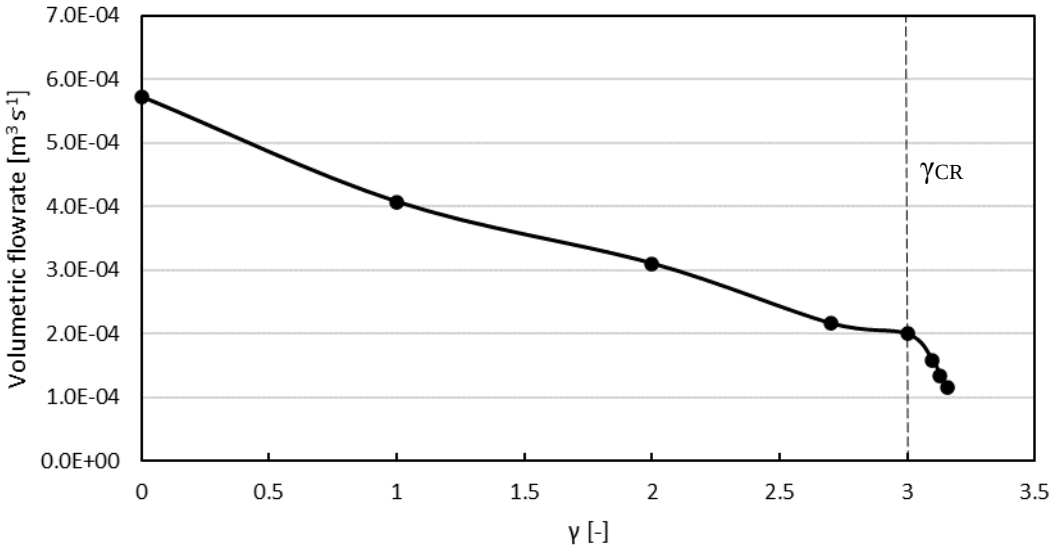

Figure 5. Volumetric blood flow with respect to γ

Transvalvular flow is another important parameter for measuring aortic valve functionality. The flow reduces as γ increases (Figure 5); it decreases almost linearly up to a critical value $\gamma_{CR} = 3$, after which it decreases sharply. In Figure 5, γ_{CR} corresponds to a flow rate of 200 ml s^{-1}. Our calculations are consistent with the medical literature where a flow rate ≥250 ml s^{-1} is considered acceptable, whereas <200 ml s^{-1} is associated with an increase of mortality rate in cases of patients with aortic stenosis [26,31]. The maximum orifice diameter and the average stress on the valve (see next section) can also be used to monitor the progression of the valve stenosis. Table 2 summarizes the parameters as the condition worsen from normal to severe.

Table 2. Parameters for determining severity of calcification

Calcification	Maximum Orifice Diameter [cm]	Mean flow $\times 10^{-4}$ [$m^3 s^{-1}$]	Average Stress [kPa]
Normal ($\gamma = 0.0$)	1.81	5.72	10.60
Mild ($\gamma = 2.0$)	1.41	3.21	91.68
Moderate ($\gamma = 2.7$)	1.29	2.17	181.61
Severe ($\gamma = 3.1$)	1.17	1.58	324.27

3.2 Stress distribution on the membrane

Calcification increases the stiffness of the valve, which results in higher stresses on the membrane. This is particularly important because mechanical stress plays a major role in the calcification of bioprostheses [32]. This, potentially, can create a vicious circle where calcification brings to higher mechanical stress, which, in turn, brings to further calcification. Figure 6 shows how the average stress increases with the degree of calcification; numerical results are consistent with those reported by Auricchio et al. (2014)[33].

Peer-reviewed version available at *ChemEngineering* **2020**, *4*, 48; doi:10.3390/chemengineering4030048

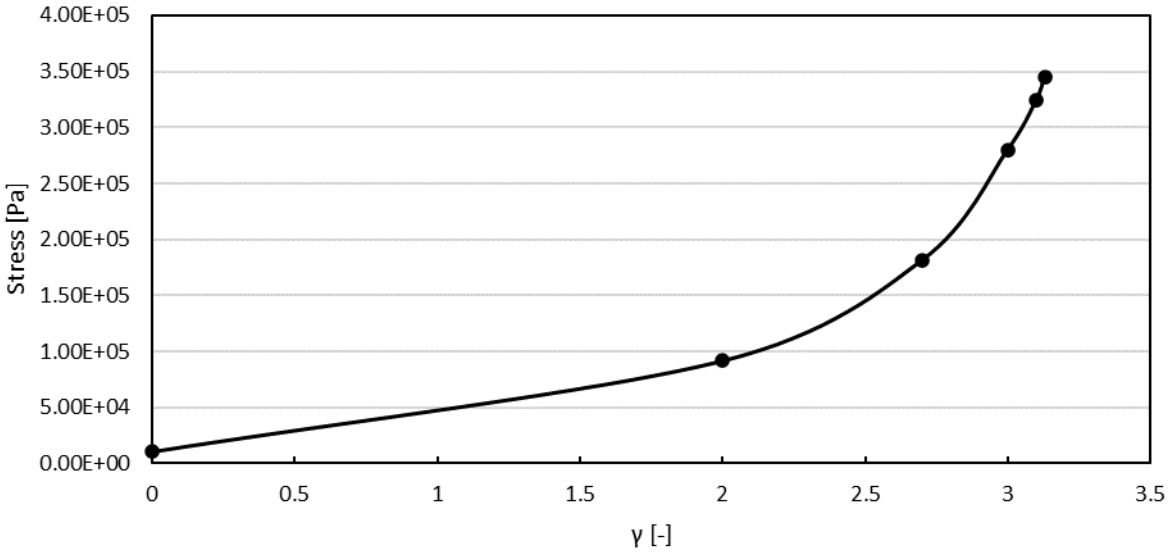

Figure 6. Stress at different degree of calcification

The local stress distribution (i.e. the Frobenius norm of the stress tensor) on the leaflets is shown in Figure 7 considering a membrane thickness of 0.6mm [7]. In this work, calcification is modelled by uniformly increasing the Young modulus of the membrane; Figure 7 suggests that calcification does not progress uniformly.

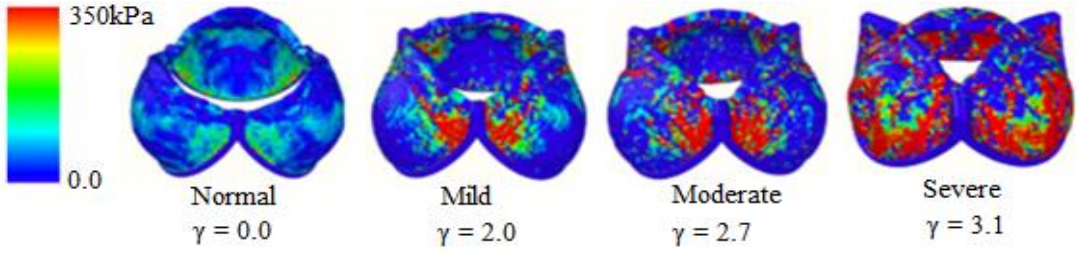

Figure 7. Mechanical stress on the valve leaflets at maximal opening.

In fact, as calcification progresses, spots of high mechanical stress appear. Firstly, they concentrate in the regions connecting two leaflets; when severe calcification is reached, they extend to the area at the basis of the valve.

4. Conclusion

In this study, the effect of calcification in a 3D aortic valve is simulated with Discrete Multi-physics. The model accounts for both hemodynamics and leaflet deformation, and it can be considered an improvement over a previous 2D model [15]. The results show that the mean transvalvular flow could be used to asses valve calcification, and severe calcification occurs when the flow rate is lower than 200 mL s^{-1}.

The model can also asses the local stress on the membrane. Calcification increases mechanical stress, which, in turn, promotes further calcification. In this work, calcification is modelled by uniformly increasing the Young modulus of the membrane. The results show that, as calcification progresses, spots of high mechanical stress appear. Firstly, they concentrate in the regions connecting two leaflets; when severe calcification is reached, they extend to the area at the basis of

the valve. This suggests that the model could be improved by accounting for local changes in stiffness, which depends on the local stress distribution.

Methodologically, this work can also benefit researchers interested in particle methods, but not necessarily to cardiovascular applications. In fact, the Appendix explains how geometries designed with CAD model can be transformed to particle models.

Author Contributions: Conceptualization**,** A.A.**,** A.M.M., and M.A.; simulation and visualization, A.M.M.; numerical calculations, A.M.M.; interpretation and analysis of results, A.M.M., and A.A; writing—original draft preparation, A.M.M.; supervision, A.A.; writing—review and editing, A.A., A.M.M and M.A.; input script, M.A. and A.A.; model and appendix, M.A. All authors have read and agreed to the published version of the manuscript.

Acknowledgement: The Nigerian Petroleum Technology Development Fund (PTDF) is acknowledged for the provision of scholarship to Adamu Musa Mohammed.

Conflicts of Interest: The authors declare no conflict of interest.

Appendix A

This explain how to adapt 3D CAD models for Discrete Multiphysics as follows: the valve geometry was initially created with the help of CAD software. In general, particle distribution can be generated with a programming code or a pre-processing solver. In the first case, the coordinates of the points are created with a separate standard programming code such as C++ and MATLAB, or directly in the processing solver with an integrated algorithm (in the software LAMMPS for instance). For complex geometries, a pre-processing commercial builder (GAMBIT, ABAQUS, SALOME) can be used for the structure and the associated mesh is then replaced with particles (Fig. A.1). In the paper, we used the second approach in order to design our tricuspid valve system.

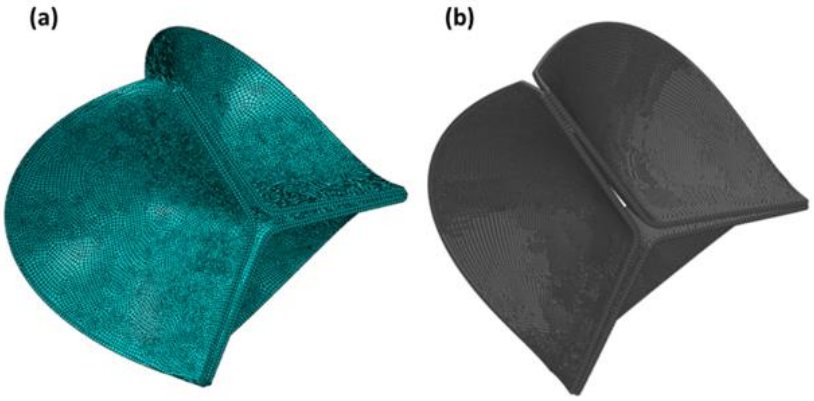

Fig. A.1. Mesh generation using a pre-processing solver (a) and the generated particle distribution (b).

The procedure of implementation is simple but requires a couple of sequences to obtain the final input file. Here, we present the one used for our valve model, but the methodology can be extended to any other applications.

The different steps can be described as follow:

1. Creation or Importation of the CAD geometry

2. Writing of the data file
3. Generation of the bond and coefficient files
4. Implementation of the input file

The first step consists of designing the part geometry or importing an existing one to any CAD commercial or open-source software (Fig. A.2a). The idea is to use the software capability for generating automatically or manually the mesh (elements and nodes, Fig. A.2b). Next, the nodes information (numbers and coordinates) are downloaded (Fig. A.2c) and collected into a text file (Fig. A.2d).

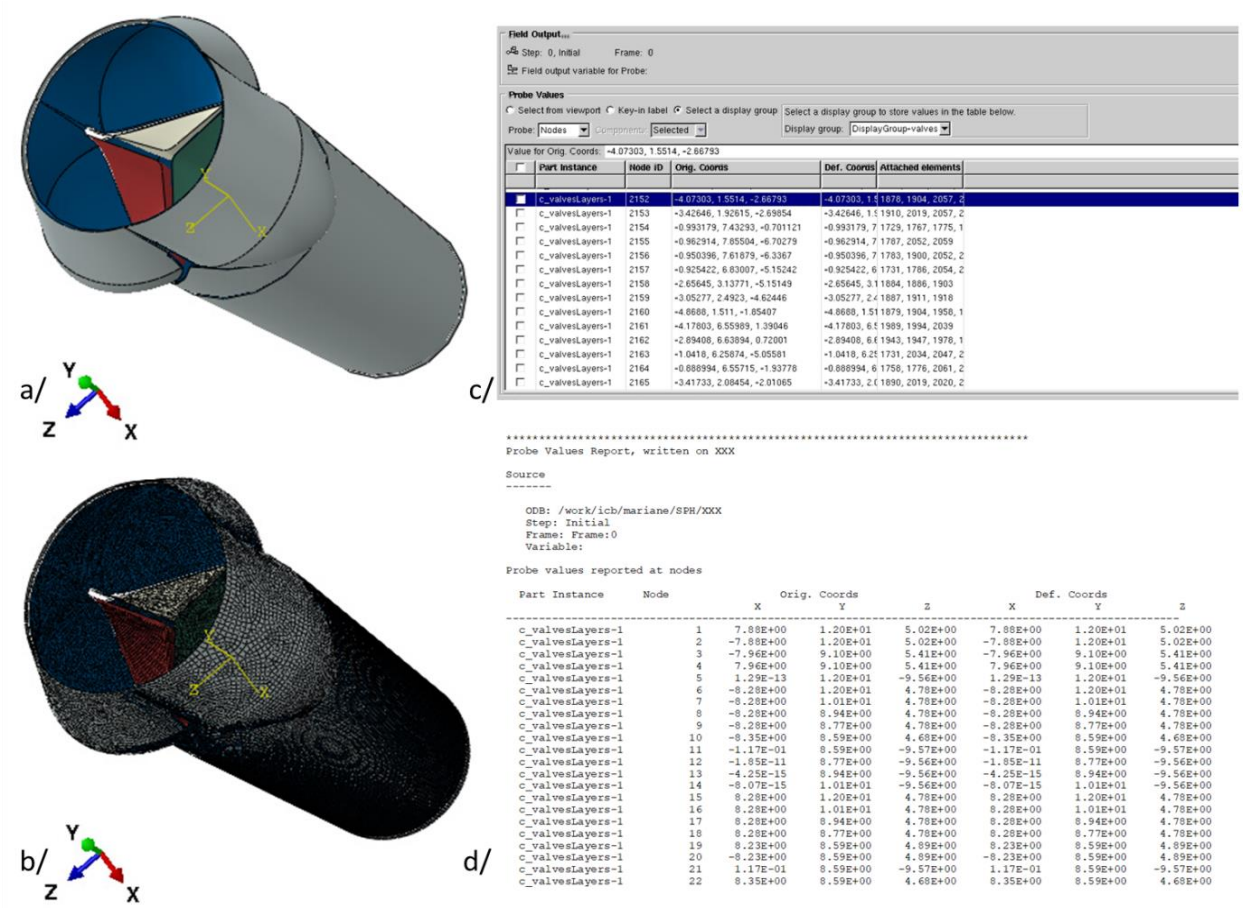

Fig. A.2. Tricuspid valve CAD part (a), tricuspid valve meshed CAD part (b), nodes generation using the CAD software (c) and external data file (d).

Subsequently, the data file is adapted and implemented in a LAMMPS format file, which contains specific line codes and keywords (for more details and documentation, readers can refer to LAMMPS documentation available at https://lammps.sandia.gov/doc/Manual.html). For instance, for this model, we used the keywords *meso* for the atom style and *bond* for the inter-atomic potential.

The unsymmetrical shape of the tricuspid valve system makes necessary a 3-D design. This representation requires a fine mesh with a consequent number of nodes (418,743 particles) to ensure a realistic valve motion. Each node/particle is connected with at least 3 other nodes located nearby, increasing drastically the data processing. As a result, we developed an algorithm (C++ code) in order to set automatically the bonds definition. All particle positions are scanned by the code and for each particle, its neighbour (within a prescribed radius distance of interaction) is identified,

numbered and printed out in a bond file. Meanwhile, a second file is also created with the storage of the bond coefficients (potential force) and the distance (between 2 particles).

Finally, as the number of fluid particles is very important (342,358), the inclusion of the list into the data file (which it is technically possible) makes heavy the input file processing. Instead, we preferred to generate, during the first step of the simulation, the fluid particles via the LAMMPS commands '*create_atoms'* and '*region*'. The command '*delete*' is also used to avoid overlapping.

References

1. Fioretta, E. S.; Dijkman, P. E.; Emmert, M. Y.; Hoerstrup, S. P. The Future of Heart Valve Replacement: Recent Developments and Translational Challenges for Heart Valve Tissue Engineering: The Future of Heart Valve Replacement. *Journal of Tissue Engineering and Regenerative Medicine* **2018**, *12* (1), e323–e335. https://doi.org/10.1002/term.2326.
2. Amindari, A.; Saltik, L.; Kirkkopru, K.; Yacoub, M.; Yalcin, H. C. Assessment of Calcified Aortic Valve Leaflet Deformations and Blood Flow Dynamics Using Fluid-Structure Interaction Modeling. *Informatics in Medicine Unlocked* **2017**, *9*, 191–199. https://doi.org/10.1016/j.imu.2017.09.001.
3. Otto, C. M.; Prendergast, B. Aortic-Valve Stenosis — From Patients at Risk to Severe Valve Obstruction. *New England Journal of Medicine* **2014**, *371* (8), 744–756. https://doi.org/10.1056/NEJMra1313875.
4. Fedele, M.; Faggiano, E.; Dedè, L.; Quarteroni, A. A Patient-Specific Aortic Valve Model Based on Moving Resistive Immersed Implicit Surfaces. *Biomechanics and Modeling in Mechanobiology* **2017**, *16* (5), 1779–1803. https://doi.org/10.1007/s10237-017-0919-1.
5. Youssefi, P.; Gomez, A.; He, T.; Anderson, L.; Bunce, N.; Sharma, R.; Figueroa, C. A.; Jahangiri, M. Patient-Specific Computational Fluid Dynamics—Assessment of Aortic Hemodynamics in a Spectrum of Aortic Valve Pathologies. *The Journal of Thoracic and Cardiovascular Surgery* **2017**, *153* (1), 8-20.e3. https://doi.org/10.1016/j.jtcvs.2016.09.040.
6. Bluestein, D.; Einav, S. The Effect of Varying Degrees of Stenosis on the Characteristics of Turbulent Pulsatile Flow through Heart Valves. *Journal of Biomechanics* **1995**, *28* (8), 915–924. https://doi.org/10.1016/0021-9290(94)00154-V.
7. Hamid, M. S.; Sabbah, H. N.; Stein, P. D. Comparison of Finite Element Stress Analysis of Aortic Valve Leaflet Using Either Membrane Elements or Solid Elements. *Computers & Structures* **1985**, *20* (6), 955–961. https://doi.org/10.1016/0045-7949(85)90015-X.
8. Arjunon, S.; Rathan, S.; Jo, H.; Yoganathan, A. P. Aortic Valve: Mechanical Environment and Mechanobiology. *Ann Biomed Eng* **2013**, *41* (7), 1331–1346. https://doi.org/10.1007/s10439-013-0785-7.
9. Morganti, S.; Conti, M.; Aiello, M.; Valentini, A.; Mazzola, A.; Reali, A.; Auricchio, F. Simulation of Transcatheter Aortic Valve Implantation through Patient-Specific Finite Element Analysis: Two Clinical Cases. *Journal of Biomechanics* **2014**, *47* (11), 2547–2555. https://doi.org/10.1016/j.jbiomech.2014.06.007.
10. Lazaros, G.; Drakopoulou, M. I.; Tousoulis, D. Transaortic Flow in Aortic Stenosis: Stroke Volume Index versus Flow Rate. *Cardiology* **2018**, *141* (1), 71–73. https://doi.org/10.1159/000494051.

11. GHASEMI BAHRASEMAN, H.; MOHSENI LANGURI, E.; YAHYAPOURJALALY, N.; ESPINO, D. M. Fluid–Structure Interaction Modeling of Aortic Valve Stenosis at Different Heart Rates. *Acta of Bioengineering and Biomechanics; 03/2016; ISSN 1509-409X* **2016**. https://doi.org/10.5277/abb-00429-2015-03.
12. Alexiadis, A. The Discrete Multi-Hybrid System for the Simulation of Solid-Liquid Flows. *PLoS ONE* **2015**, *10* (5), e0124678. https://doi.org/10.1371/journal.pone.0124678.
13. Alexiadis, A. A Smoothed Particle Hydrodynamics and Coarse-Grained Molecular Dynamics Hybrid Technique for Modelling Elastic Particles and Breakable Capsules under Various Flow Conditions: SPH-CGMD HYBRID. *Int. J. Numer. Meth. Engng* **2014**, *100* (10), 713–719. https://doi.org/10.1002/nme.4782.
14. Alexiadis, A. A New Framework for Modelling the Dynamics and the Breakage of Capsules, Vesicles and Cells in Fluid Flow. *Procedia IUTAM* **2015**, *16*, 80–88. https://doi.org/10.1016/j.piutam.2015.03.010.
15. Ariane, M.; Allouche, M. H.; Bussone, M.; Giacosa, F.; Bernard, F.; Barigou, M.; Alexiadis, A. Discrete Multi-Physics: A Mesh-Free Model of Blood Flow in Flexible Biological Valve Including Solid Aggregate Formation. *PLoS ONE* **2017**, *12* (4), e0174795. https://doi.org/10.1371/journal.pone.0174795.
16. Alexiadis, A.; Stamatopoulos, K.; Wen, W.; Batchelor, H. K.; Bakalis, S.; Barigou, M.; Simmons, M. J. H. Using Discrete Multi-Physics for Detailed Exploration of Hydrodynamics in an in Vitro Colon System. *Computers in Biology and Medicine* **2017**, *81*, 188–198. https://doi.org/10.1016/j.compbiomed.2017.01.003.
17. Ariane, M.; Vigolo, D.; Brill, A.; Nash, F. G. B.; Barigou, M.; Alexiadis, A. Using Discrete Multi-Physics for Studying the Dynamics of Emboli in Flexible Venous Valves. *Computers & Fluids* **2018**, *166*, 57–63. https://doi.org/10.1016/j.compfluid.2018.01.037.
18. Ariane, M.; Wen, W.; Vigolo, D.; Brill, A.; Nash, F. G. B.; Barigou, M.; Alexiadis, A. Modelling and Simulation of Flow and Agglomeration in Deep Veins Valves Using Discrete Multi Physics. *Computers in Biology and Medicine* **2017**, *89*, 96–103. https://doi.org/10.1016/j.compbiomed.2017.07.020.
19. Ariane, M.; Kassinos, S.; Velaga, S.; Alexiadis, A. Discrete Multi-Physics Simulations of Diffusive and Convective Mass Transfer in Boundary Layers Containing Motile Cilia in Lungs. *Computers in Biology and Medicine* **2018**, *95*, 34–42. https://doi.org/10.1016/j.compbiomed.2018.01.010.
20. Alexiadis, A. Deep Multiphysics: Coupling Discrete Multiphysics with Machine Learning to Attain Self-Learning in-Silico Models Replicating Human Physiology. *Artificial Intelligence in Medicine* **2019**, *98*, 27–34. https://doi.org/10.1016/j.artmed.2019.06.005.
21. Liu, G. R.; Liu, M. B. *Smoothed Particle Hydrodynamics: A Meshfree Particle Method*; World Scientific: New Jersey, 2003.
22. Kot, M.; Nagahashi, H.; Szymczak, P. Elastic Moduli of Simple Mass Spring Models. *Vis Comput* **2015**, *31* (10), 1339–1350. https://doi.org/10.1007/s00371-014-1015-5.
23. Plimpton, S. Fast Parallel Algorithms for Short-Range Molecular Dynamics. *Journal of Computational Physics* **1995**, *117* (1), 1–19. https://doi.org/10.1006/jcph.1995.1039.

24. Stevens, S. A.; Lakin, W. D.; Goetz, W. A Differentiable, Periodic Function for Pulsatile Cardiac Output Based on Heart Rate and Stroke Volume. *Mathematical Biosciences* **2003**, *182* (2), 201–211. https://doi.org/10.1016/S0025-5564(02)00200-6.
25. Murgo, J. P.; Westerhof, N.; Giolma, J. P.; Altobelli, S. A. Aortic Input Impedance in Normal Man: Relationship to Pressure Wave Forms. *Circulation* **1980**, *62* (1), 105–116. https://doi.org/10.1161/01.CIR.62.1.105.
26. Blais, C.; Burwash, I. G.; Mundigler, G.; Dumesnil, J. G.; Loho, N.; Rader, F.; Baumgartner, H.; Beanlands, R. S.; Chayer, B.; Kadem, L.; Garcia, D.; Durand, L.-G.; Pibarot, P. Projected Valve Area at Normal Flow Rate Improves the Assessment of Stenosis Severity in Patients With Low-Flow, Low-Gradient Aortic Stenosis: The Multicenter TOPAS (Truly or Pseudo-Severe Aortic Stenosis) Study. *Circulation* **2006**, *113* (5), 711–721. https://doi.org/10.1161/CIRCULATIONAHA.105.557678.
27. Hammer, P. E.; Sacks, M. S.; del Nido, P. J.; Howe, R. D. Mass-Spring Model for Simulation of Heart Valve Tissue Mechanical Behavior. *Ann Biomed Eng* **2011**, *39* (6), 1668–1679. https://doi.org/10.1007/s10439-011-0278-5.
28. Pazdniakou, A.; Adler, P. M. Lattice Spring Models. *Transp Porous Med* **2012**, *93* (2), 243–262. https://doi.org/10.1007/s11242-012-9955-6.
29. Lloyd, B.; Szekely, G.; Harders, M. Identification of Spring Parameters for Deformable Object Simulation. *IEEE Trans. Visual. Comput. Graphics* **2007**, *13* (5), 1081–1094. https://doi.org/10.1109/TVCG.2007.1055.
30. Kamimura, D.; Hans, S.; Suzuki, T.; Fox, E. R.; Hall, M. E.; Musani, S. K.; McMullan, M. R.; Little, W. C. Delayed Time to Peak Velocity Is Useful for Detecting Severe Aortic Stenosis. *JAHA* **2016**, *5* (10). https://doi.org/10.1161/JAHA.116.003907.
31. Saeed, S.; Senior, R.; Chahal, N. S.; Lønnebakken, M. T.; Chambers, J. B.; Bahlmann, E.; Gerdts, E. Lower Transaortic Flow Rate Is Associated With Increased Mortality in Aortic Valve Stenosis. *JACC: Cardiovascular Imaging* **2017**, *10* (8), 912–920. https://doi.org/10.1016/j.jcmg.2017.05.008.
32. Thubrikar, M.; Deck, J.; Aouad, J.; Nolan, S. Role of Mechanical Stress in Calcification of Aortic Bioprosthetic Valves. *The Journal of thoracic and cardiovascular surgery* **1983**, *86* (1), 115—125.
33. Auricchio, F.; Conti, M.; Morganti, S.; Reali, A. Simulation of Transcatheter Aortic Valve Implantation: A Patient-Specific Finite Element Approach. *Computer Methods in Biomechanics and Biomedical Engineering* **2014**, *17* (12), 1347–1357. https://doi.org/10.1080/10255842.2012.746676.